Science
AAAS

Supplementary Materials for

Structure, mechanism, and regulation of the chloroplast ATP synthase

Alexander Hahn, Janet Vonck, Deryck J. Mills, Thomas Meier*, Werner Kühlbrandt*

Correspondence to: werner.kuehlbrandt@biophys.mpg.de (WK), t.meier@imperial.ac.uk (TM)

This PDF file includes:

Figures S1-S13

Table S1

References (*69-78*)

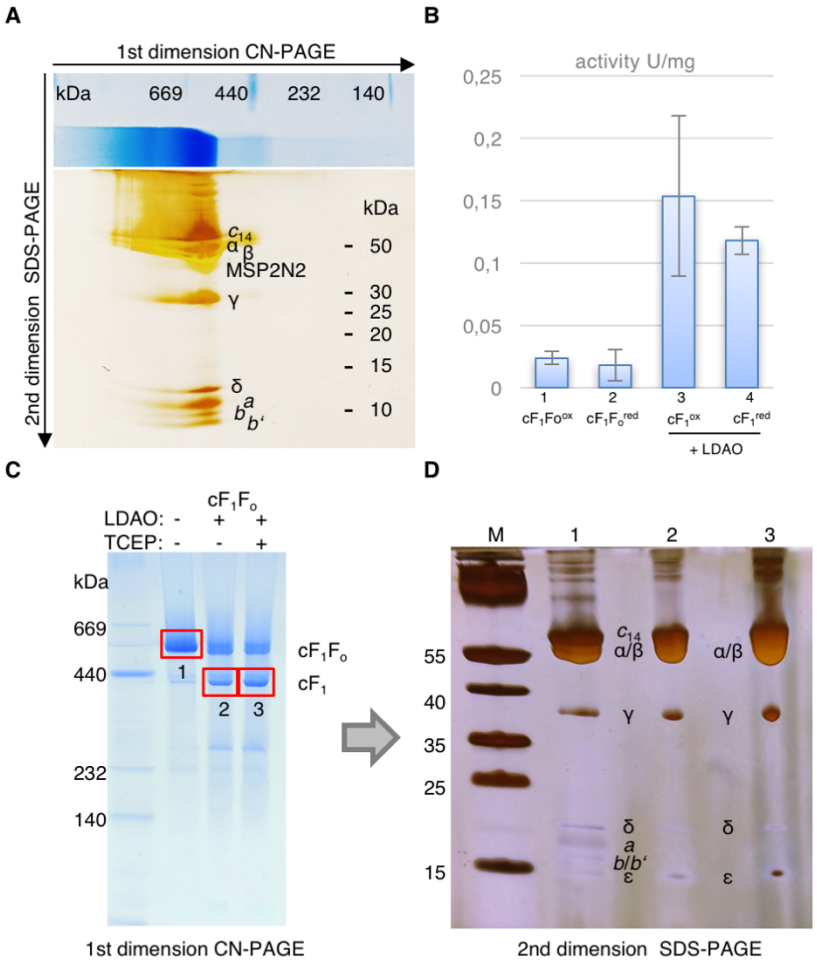

Fig. S1

Purification, nanodisc reconstitution and hydrolytic activity of cF_1F_o. cF_1F_o was purified from market spinach and reconstituted into lipid nanodiscs (see Materials and Methods for details). **A**, The cF_1F_o complex is intact and highly pure as demonstrated by two-dimensional gel electrophoresis. The complex migrates at ~550 kDa in clear-native PAGE (Coomassie-stained). SDS-PAGE in the second dimension (silver-stained) dissociates all cF_1F_o subunits except the c_{14}-ring that migrates above subunit α. The nanodisc protein MSP2N2 migrates at 45 kDa. Molecular weights in kDa are indicated. **B**, The ADP-inhibited cF_1F_o complex shows only residual hydrolytic activity in the mU/mg range and is insensitive to reduction by 5 mM TCEP (1, 2). ATP hydrolysis is activated by addition of 0.1% (v/v) LDAO (3, 4). **C**, Clear-native PAGE of cF_1F_o treated with TCEP and LDAO for activity measurements in (B). LDAO partially dissociates cF_o from cF_1. Activation of *E. coli* ATPase by LDAO is attributed to a change in the interaction of ε subunit with subunit β (*69*). Red boxes indicate samples 1-3 analyzed by second-

dimension SDS-PAGE in (D). **D**, cF_1F_o in sample 1 contains all F_1 and F_o subunits (*a*, *b*, *b*' and c_{14} ring). Samples 2 and 3 contain cF_1 subunits α, β, γ, δ and ε, but not F_o.

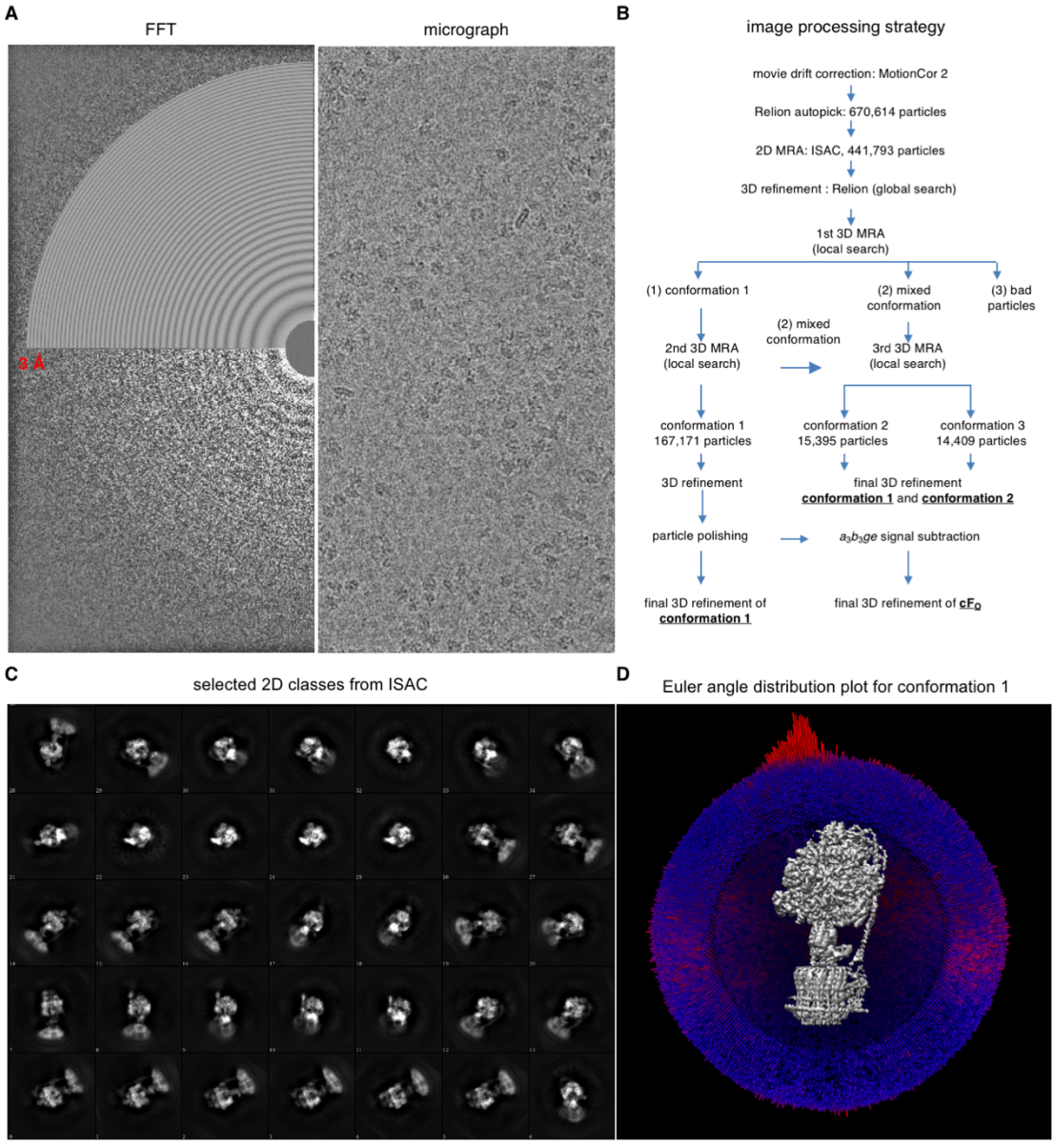

Fig. S2

Image quality and processing. A, Dose-fractionated movies were collected automatically in a Titan Krios with a Falcon III direct electron detector. Drift between movie frames was corrected by MotionCor2. cF_1F_o particles are readily visible and evenly distributed. The FFT of most images indicated signal to ~3 Å. (**B**) Image processing strategy. (**C**) Selected 2D classes sorted by ISAC. Classes show a wide distribution of equally populated orientations. (**D**) Plot of Euler angle distribution for particles in conformation 1.

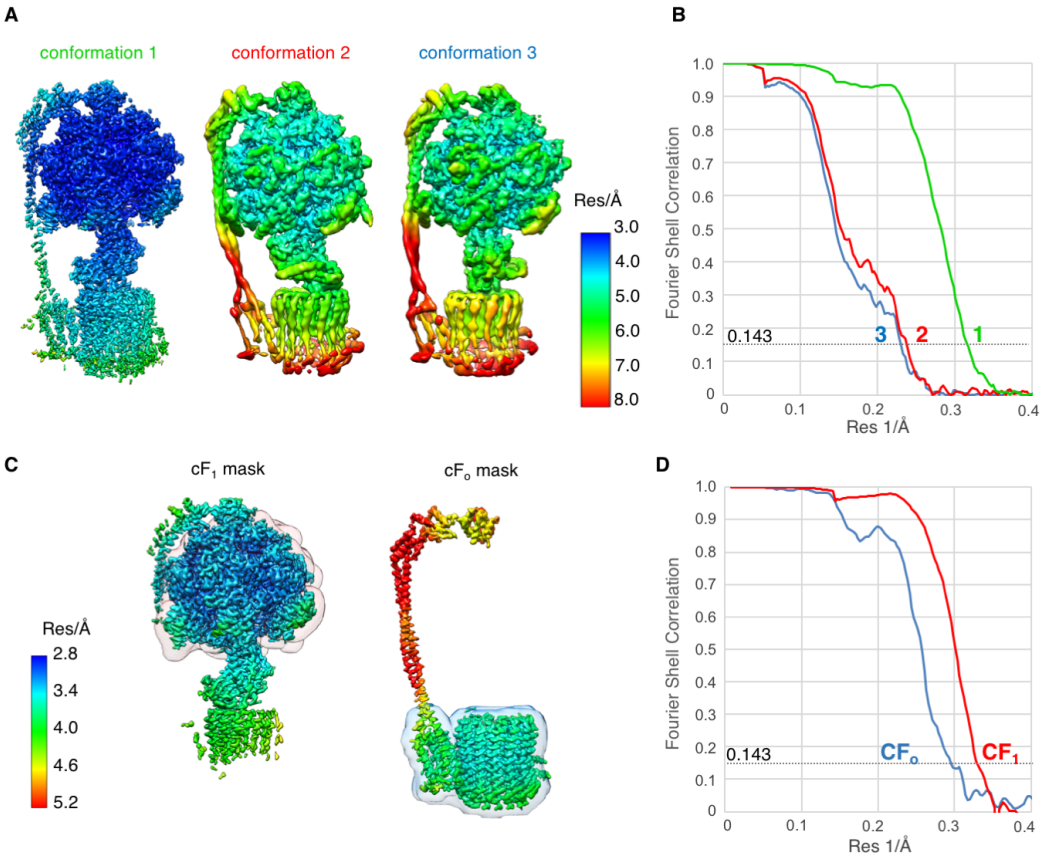

Fig. S3

Global and local resolution estimates. (**A**) 3D maps of rotary states in the three main particle classes were reconstructed with Relion 2.1. In all three maps cF_1 is better defined than cF_o. Local resolution anisotropy (red to green) was estimated with Relion 2.1. (**B**) Fourier shell correlation (FSC). Resolution was determent for the complete reconstruction of conformations 1, 2 and 3. Conformation 1 has the highest number of particles and attains an overall resolution of 3.15 Å, as estimated by FSC 0.143 (*70*). Particles in Class 2 and 3 were refined to 4.2 and 4.3 Å resolution, respectively. (**C**) FSC of masked cF_1 (red) and cF_o (blue). For cF_o reconstruction, the $\alpha_3\beta_3\gamma\varepsilon$ signal was subtracted from the particle images to improve cF_o alignment. Local resolution anisotropy (red to green) was estimated with Relion 2.1. (**D**) FSC 0.143 resolution determination of masked cF_1 and cF_o as shown in (C). The average resolution of the masked cF_1 and cF_o reconstructions converged at 3.05 Å and 3.38 Å, respectively.

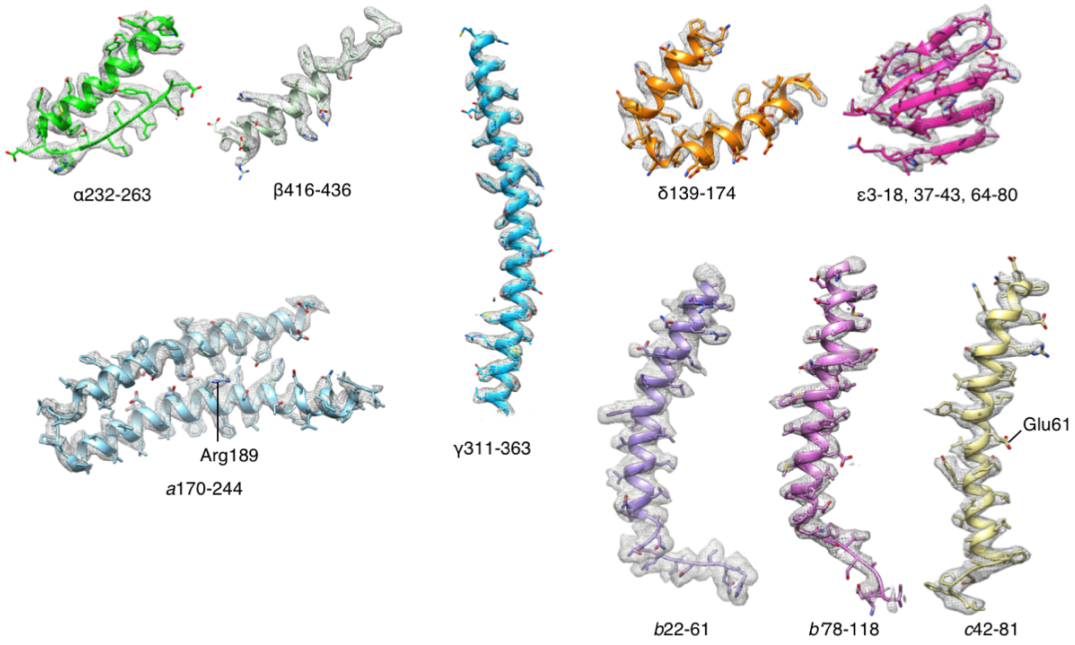

Fig. S4

Examples of atomic models built in the cryo-EM map. Examples of density and model are shown for each subunit. The range of amino acids shown is indicated for each subunit.

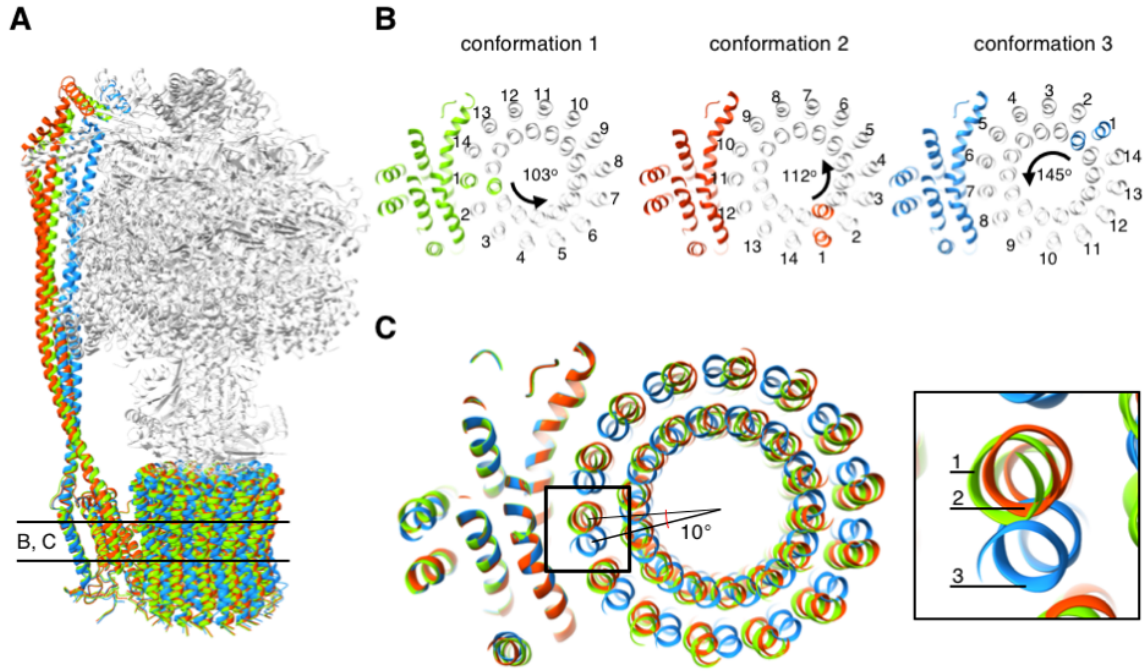

Fig. S5

Orientation of the c-ring. (**A**) Superimposed models for conformations 1, 2 and 3 aligned on subunit *a*. Subunits *abb'c*$_{14}$ are colored by conformation (1, green; 2, red; 3, blue). (**B**) Rotation angles between conformations are indicated. (**C**) Cross-section of superimposed cF$_o$ conformations as indicated in (A). *c*-ring subunit positions in conformations 1 and 2 are similar; conformation 3 is offset by ~10°, corresponding to almost one half of a *c*-subunit.

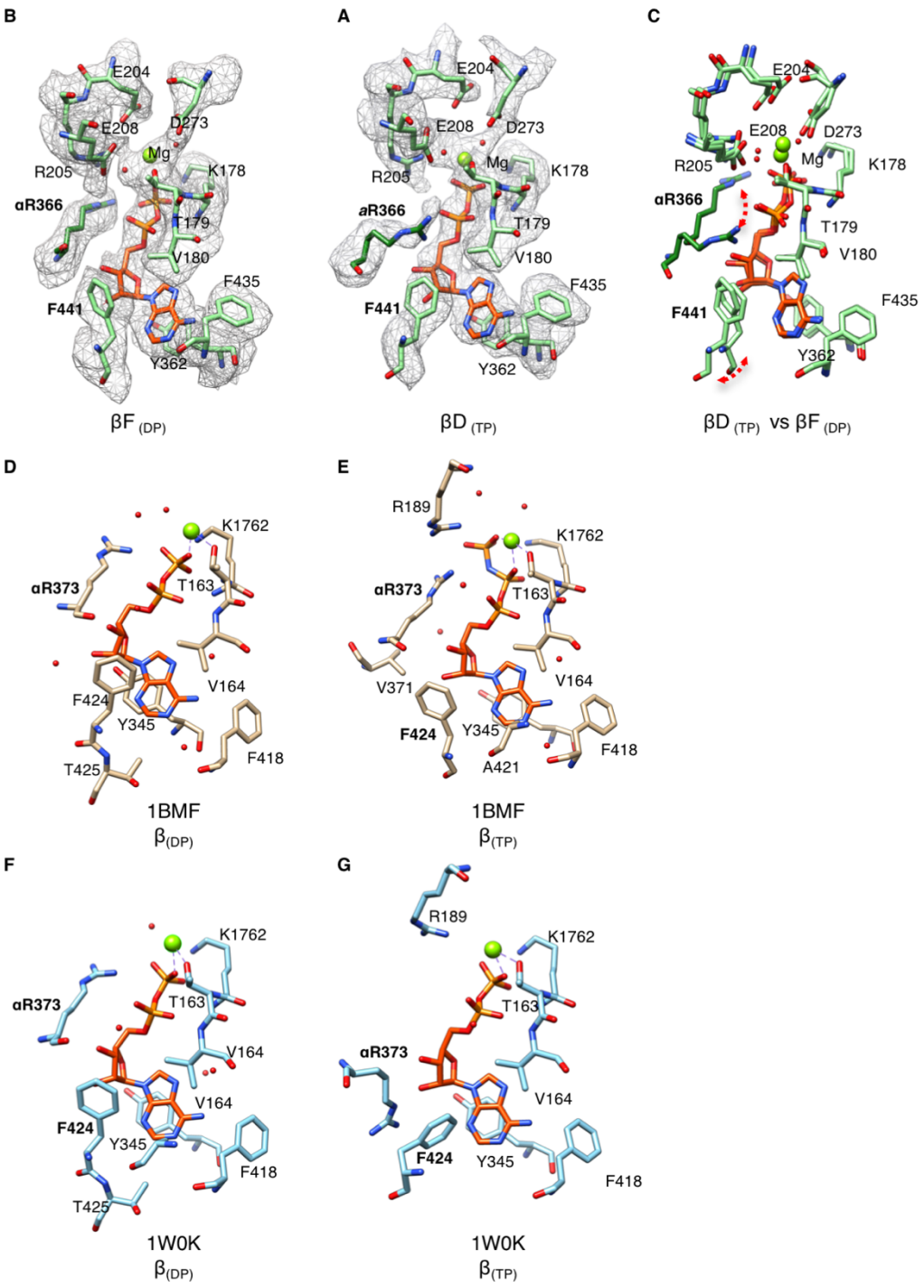

Fig. S6

Nucleotide-binding sites in subunit β_{TP} and β_{DP}. (**A**) Mg-ADP in the β_{DP} site of β-subunit F and (**B**) the β_{TP} site of β-subunit D with adjacent residues fitted to the cryo-EM density filtered to 2.9 Å. Mg ions (green) and coordinating water molecules (red) are resolved. The overlay of the two models (**C**) shows significant differences in sidechain orientation of αArg366 and position of βPhe441 (red dashed arrows). Interestingly, whereas as in other high-resolution cryo-EM structures (*71, 72*) the carboxylate groups of most acidic sidechains are absent due to electron

irradiation, the sidechains of βAsp273 and βGlu208, which coordinate the water molecules, are well-resolved. Carboxylates with good density in cryo-EM maps are usually involved in ligand binding or strong salt bridges (*73*). Apparently, carboxylate groups in this chemical environment are more resistant to radiation damage.

The F_1 nucleotide-binding sites are highly conserved throughout evolution; the α and β subunits of cF_1 respectively share 58 and 67% sequence identity with their mitochondrial counterparts, and the residues forming the nucleotide binding sites are identical (*25*). (**D**) In F_1 from bovine mitochondria (PDB ID 1BMF) (*28*), the β_{DP} site contains ADP and is similar to cF_1. (**E**) the β_{TP} site contains the inhibitor AMP-PNP that was added for crystallization. The residue equivalent to αArg366 (αArg373) is oriented towards the γ-phosphate. Similar changes in sidechain conformation of this conserved arginine in the β_{TP} site were observed in bovine F_1 when all five sites were occupied by ADP (PDB ID 1W0K) (*74*) and were taken to result from the absence of a γ-phosphate in the βTP site. ADP molecules and Mg ions, each with two coordinating water molecules, are visible in both the β_{DP} (**F**) and the β_{TP} site (**G**).

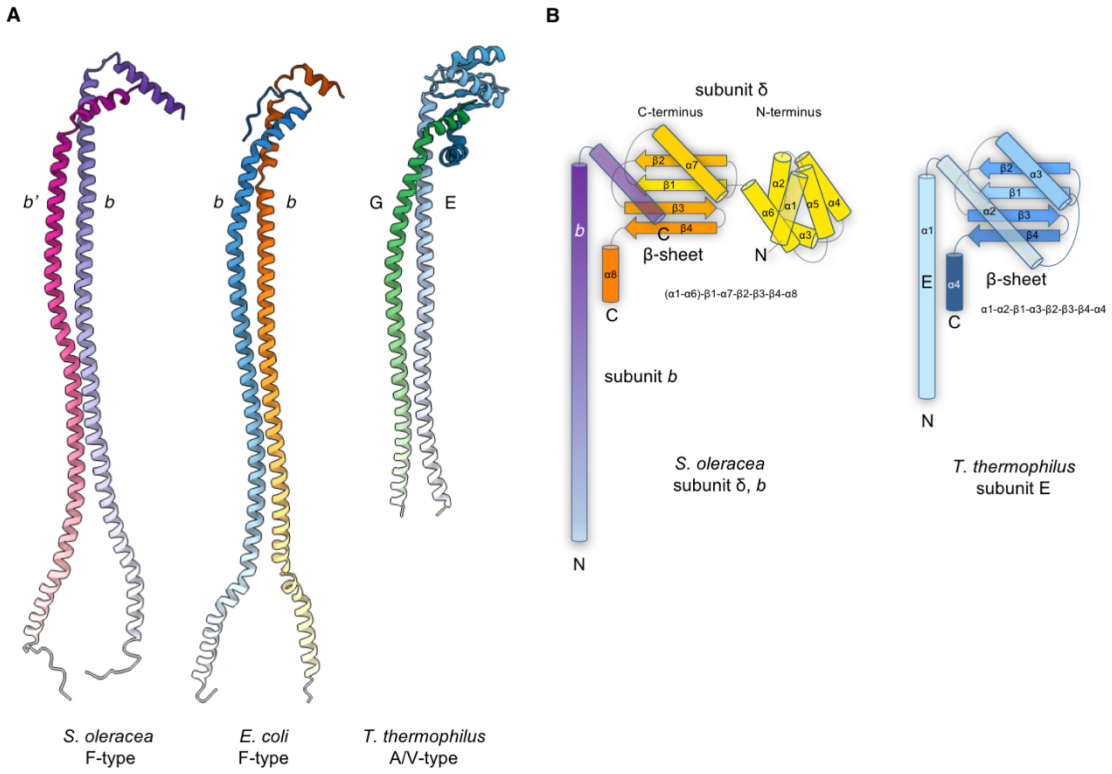

Fig. S7.

Arrangement and conservation of the peripheral stalk in rotary ATPases. (**A**) Subunits *b* and *b*' form a right-handed coiled coil. This arrangement is conserved in all rotary ATPases, including the *b*-subunits of F-type ATP synthase from *Escherichia coli* (PDB ID 5TQ4) (*18*) and the heterodimeric outer stalk of the distantly related A/V-type ATPase from *Thermus thermophilus* (PDB ID 3V6I) (*32*). (**B**) The peripheral stalk is attached to cF_1 by the subunit δ (OSCP in mitochondria), the C-terminal domain of which consists of a mixed β-sheet fold. This fold is conserved in the C-terminal domain of the peripheral stalk subunit E of the *T. thermophilus* A-type ATPase. The N-terminus of E corresponds to *b* in cF_1F_o (A). The N-terminal domain of δ is absent in A-type ATPases, which have a different architecture than F_1F_o with two EG peripheral stalks (*75*), supporting the notion that subunit δ ensures the attachment of only one peripheral stalk to F_1.

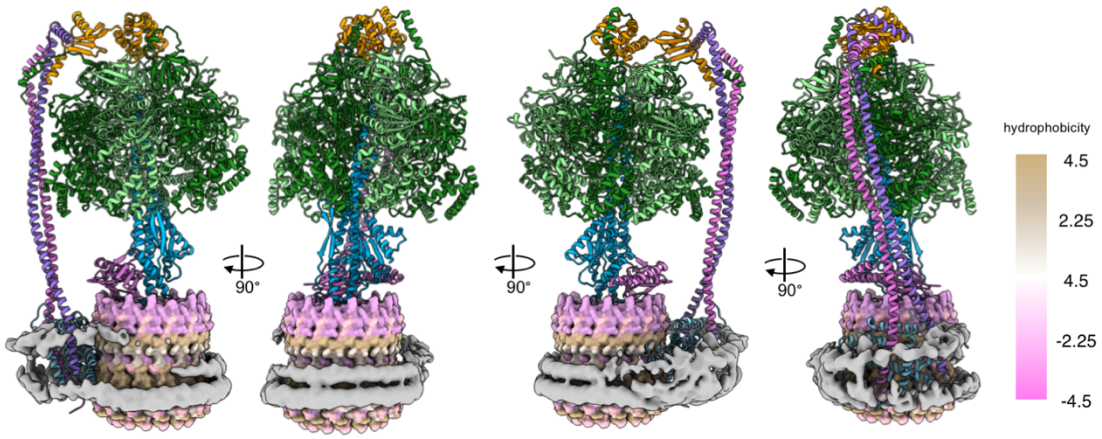

Fig. S8

cF_1-F_o in lipid nanodiscs. The membrane scaffold protein (MSP; grey density) wraps around and stabilizes the membrane-embedded cF_o subcomplex. MSP forms a horizontal double belt of α-helices that are well-defined at the *c*-ring/membrane interface but disordered near subunits *a, b* and *b*'. Hydrophobicity of the *c*-ring is shown in the Kyte-Doolittle scale with colors ranging from pink for the most hydrophilic to white at 0.0 to tan for the most hydrophobic (*76*). We see no density for lipid molecules in the map.

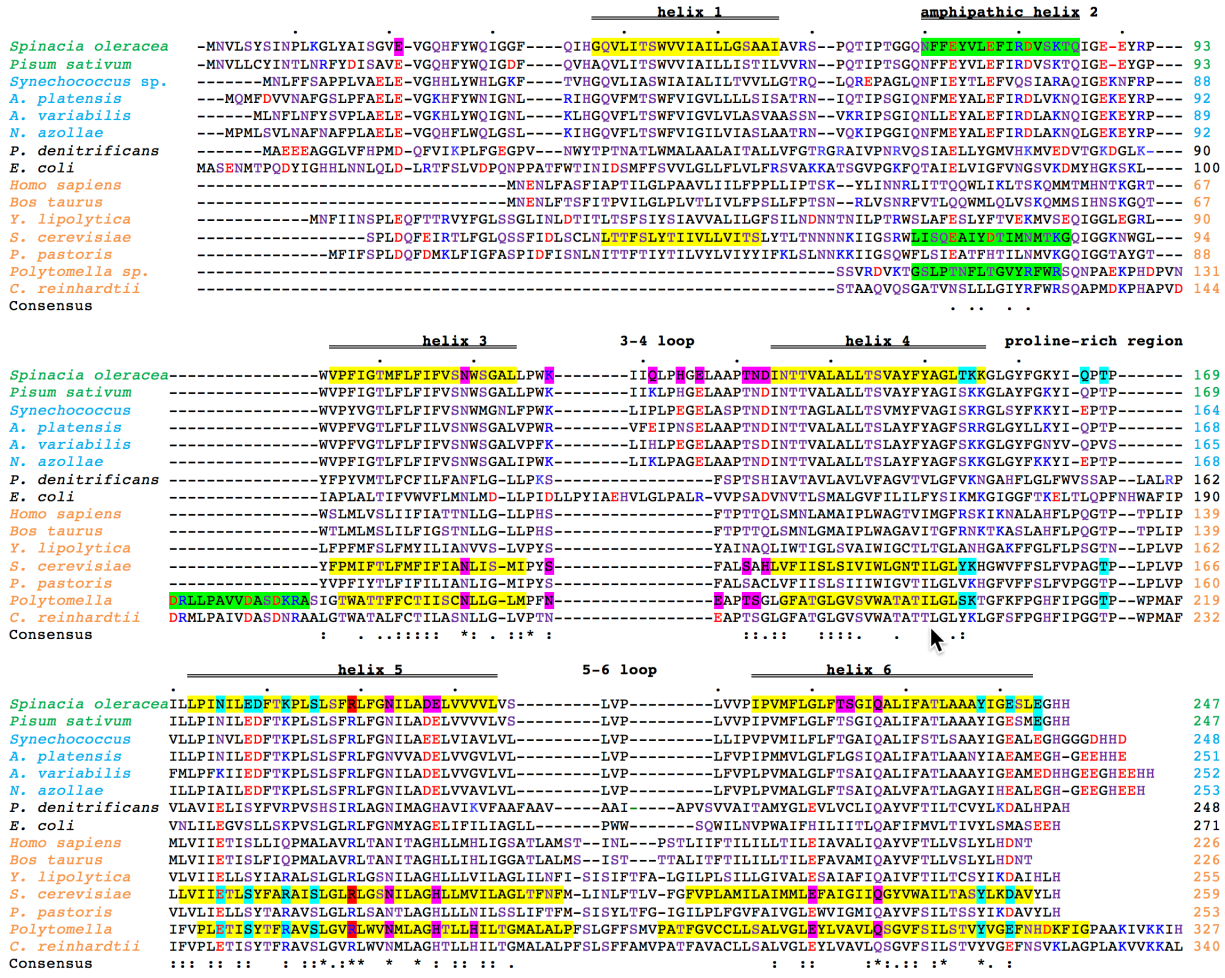

Fig. S9

Structure-based sequence alignment of ATP synthase subunit *a*. Sequences are from chloroplasts (green font), cyanobacteria (cyan font), other bacteria (black font) and mitochondria (orange font). Yellow highlights mark membrane-embedded helices H1, H3/4 and H5/6 in spinach chloroplasts (this work) or *Polytomella* (*9*) and yeast (*10*) mitochondria. Amphipathic surface helices are highlighted in green. Red highlight: strictly conserved arginine; purple and cyan highlights, polar residues in the proton access and exit channels. Red font, negatively charged residues (aspartate and glutamate); blue font, positively charged residues (lysine and arginine); purple font, polar residues (asparagine, glutamine, serine, threonine, histidine). Consensus: (*), strictly conserved; (:), highly conserved; (.), similar.

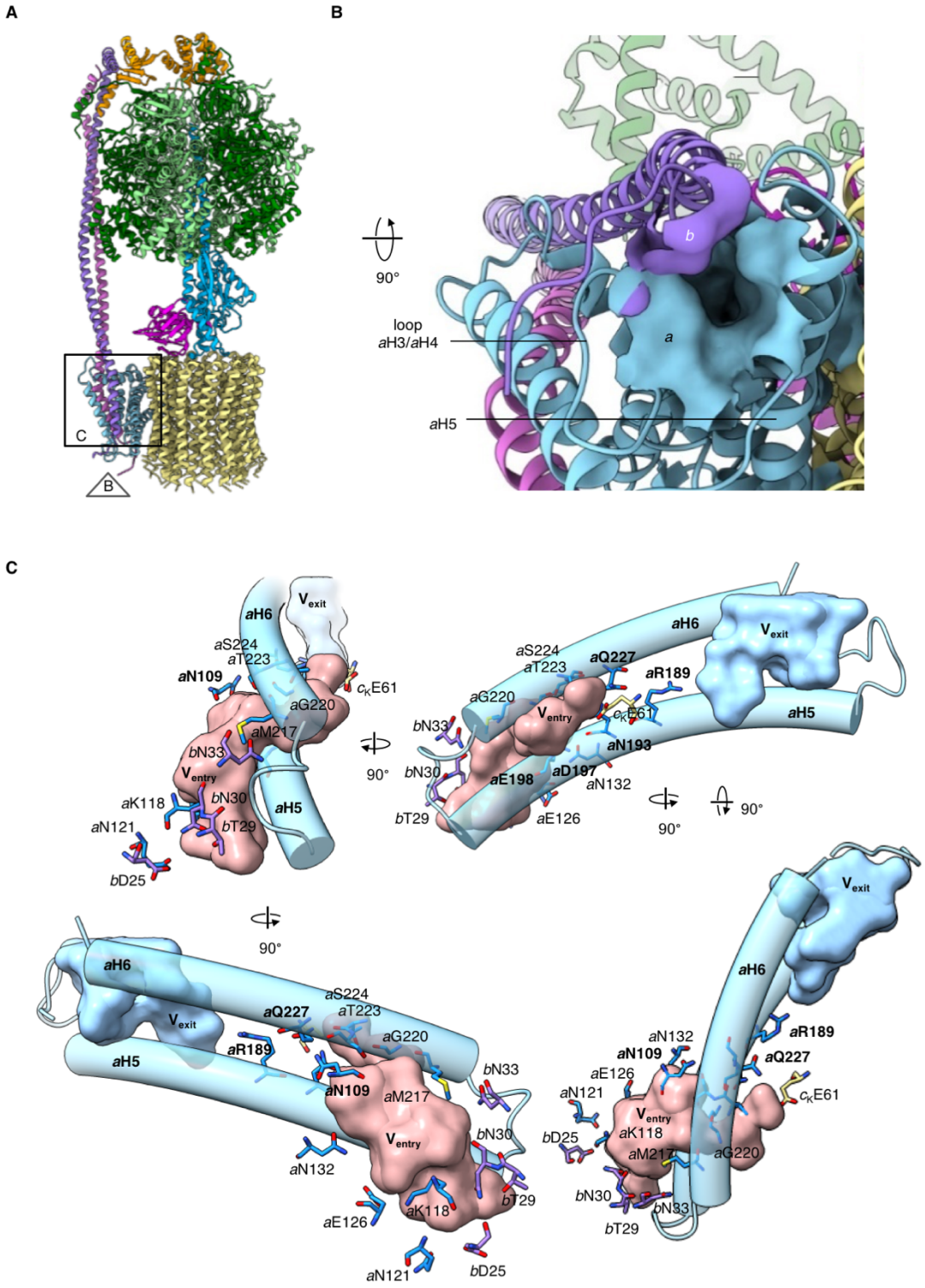

Fig. S10

The lumenal proton entry channel. (A) Overview of cF_1F_o with channel position indicated. **(B)** View into the proton entry channel from the lumen as indicated in (A). Water-accessible cavities at the subunit a/c_{14}-ring interface were mapped with HOLLOW (*66*). Residues of subunits *a* and

b within 3 Å of the mapped channel are shown in surface representation. The entry channel is formed by *a*H5 and *a*H6, the long *a*H3-*a*H4-loop and some subunit *b* residues. (**C**) View from the membrane plane (slightly slanted, from the side of the *c*-ring) (top panel) and view perpendicular to the membrane from the stroma (lower panel). Charged and polar residues defining the aqueous channel (light red) are shown in stick representation. Strictly conserved residues are labelled bold. The water-filled channel passes between the long *a*H5-*a*H6 hairpin at residues Asp197 and Glu198 and ends at the conserved *c*-ring glutamate *c*Glu61. Amino acid residues are colored according to subunit identity (subunit *a*, blue; subunit *b*, magenta). The arrow indicates the direction of *c*-ring rotation in ATP synthesis mode, with the *c*E61 residues (red) passing the aqueous channel.

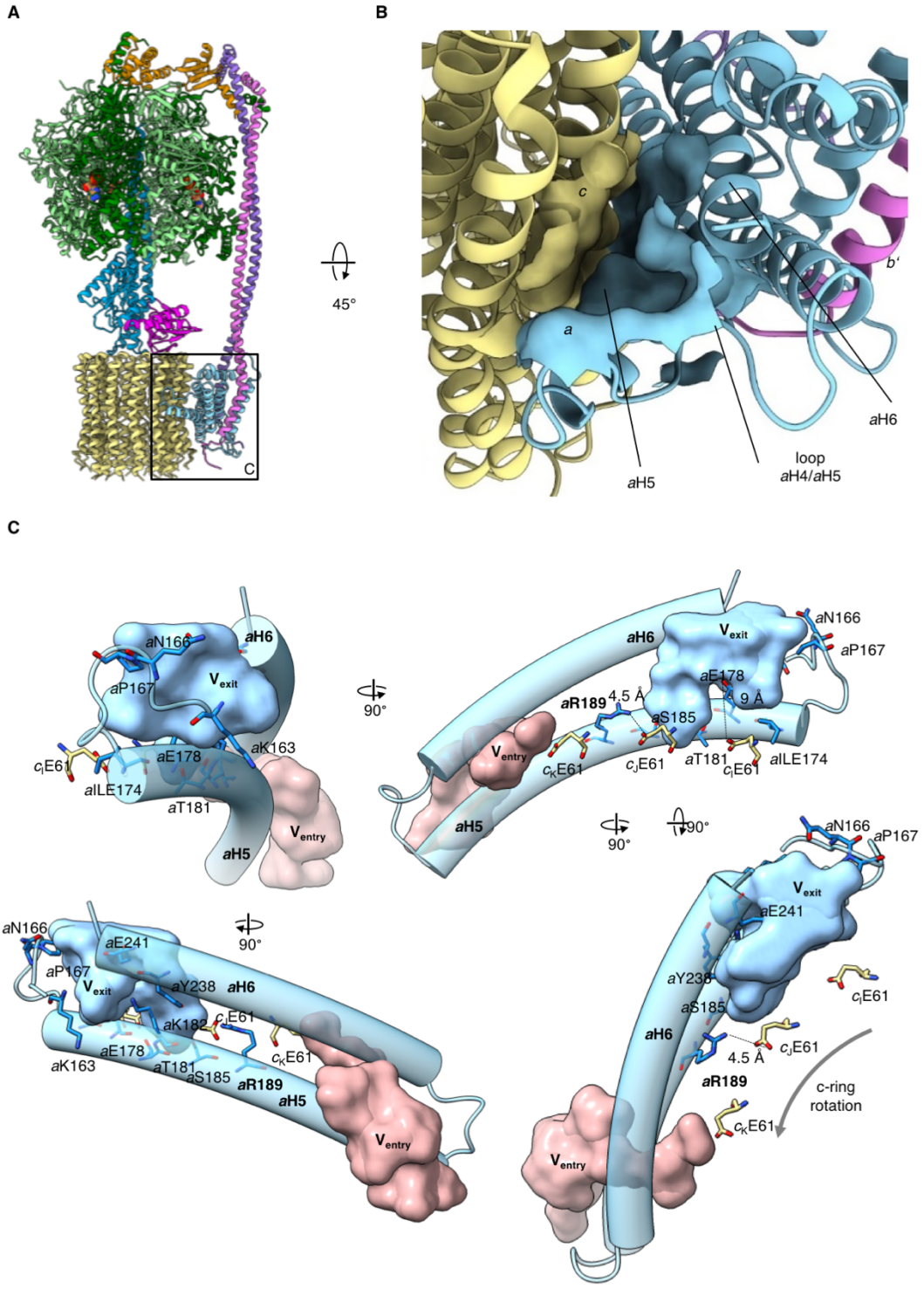

Fig. S11

The stromal proton exit channel. (**A**) Overview of cF_1F_o indicating position of stromal proton exit channel (red box). (**B**) View into the proton exit channel from the stroma. Water-accessible cavities at the subunit a/c_{14}-ring interface were mapped with HOLLOW (*66*). Residues within 3 Å of the mapped channel are shown in surface representation. The exit channel is formed by the

proline-rich loop between *a*H4-*a*H5, *a*H5, *a*H6 and the *c*-ring. (**C**) View of the exit channel from the *c*-ring. Charged and polar residues that form the mapped water-filled cavity (light blue) are shown in stick representation. The cavity runs along the subunit *a*/*c*-ring interface and ends at the strictly conserved *a*Arg189. Protonated *c*-ring glutamates rotating out of the hydrophobic lipid phase enter the aqueous phase and deprotonate. Amino acid residues are colored according to subunit identity (subunit *a*, blue; subunit *c*, pale yellow).

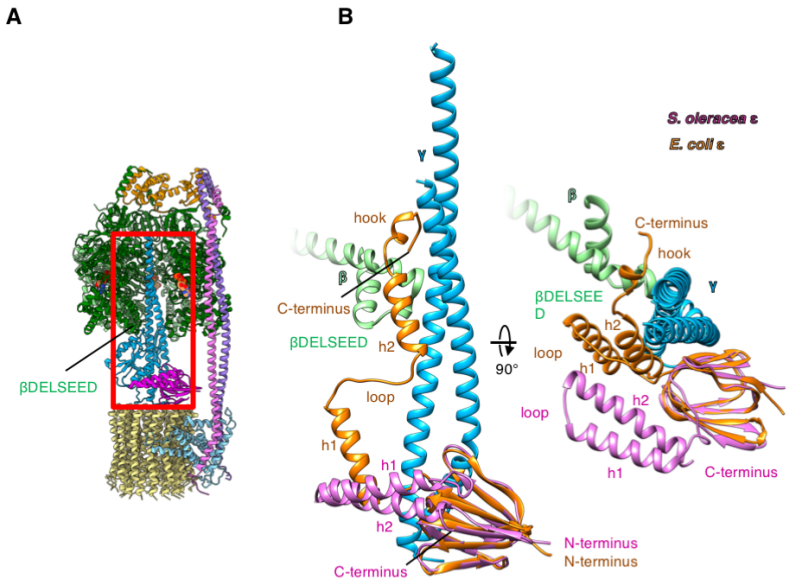

Fig. S12

cF_1F_o is not inhibited by subunit ε. (**A**) Overview showing subunit ε (pink) next to subunit γ (blue). Subunits αE and βF are omitted for clarity. The red box indicates the γε rotor. (**B**) Detailed side view (left) and top view (right) of the γε rotor within the F_1 head. The C-terminal domain of subunit ε in spinach cF_1F_o (pink) has two short α-helices forming a hairpin next to the N-terminal antiparallel β-barrel. In bacteria, two C-terminal helices h1 and h2 of subunit ε (orange, PDB ID: 3OAA (*42*) extend along the γ-subunit rotor (*77, 78*), and inhibit ATP hydrolysis through interaction of h2 and the hook domain with the DELSEED motif of subunit β (light green). In cF_1F_o, h1 and h2 cannot interact with subunit β and thus do not inhibit ATP hydrolysis.

Fig. S13

Sequence alignment of ATP synthase subunit γ. Comparison of sequences from chloroplasts (green font), cyanobacteria (cyan font) and mitochondria (orange font). Green, α-helices; yellow, β-strands. Cyanobacteria and chloroplast γ subunits have a ~30 residue regulatory insert in front of the C-terminal α-helix (consensus in cyan); chloroplasts have nine more residues (consensus in cyan) forming a β-hairpin with two conserved cysteines (red font) that can form a disulfide bond. Consensus: (*), strictly conserved; (:), highly conserved; (.), similar.

Table S1.
Cryo-EM data collection, refinement and validation statistics

	Conformation 1 (EMDB-4270) (PDB ID 6FKF)	Conformation 2 (EMDB-4271) (PDB ID 6FKH)	Conformation 3 (EMDB-4272) (PDB ID 6FKI)
Data collection and processing			
Electron microscope	Titan Krios	Titan Krios	Titan Krios
Electron detector	Falcon III	Falcon III	Falcon III
Magnification	75,000	75,000	75,000
Voltage (kV)	300	300	300
Electron exposure (e^{-}/Å^2)	25	25	25
Defocus range (μm)	1.5-2.5	1.5-2.5	1.5-2.5
Pixel size (Å)	1.053	1.053	1.053
Symmetry imposed	C1	C1	C1
Initial particle images (no.)	670,614	670,614	670,614
Final particle images (no.)	167,171	15,395	14,409
Map resolution (Å)	3.1	4.2	4.3
FSC threshold	0.143	0.143	0.143
Map resolution range (Å)	2.9-3.8	4-8	4-8
Map sharpening *B* factor (Å^2)	-150	-163	-167
Model building and refinement			
Initial models used (PDB ID)	1KMH, 5HKK, 2RQ7, 2A7U, 3C3V	6FKF	6FKF
Model composition			
Protein chains	26		
Protein residues	5201		
Ligands	3 Mg-ATP, 2 Mg-ADP		
R.m.s. deviations			
Bond lengths (Å)	0.017		
Bond angles (°)	1.25		
Ramachandran plot			
Favored (%)	96.23		
Disallowed (%)	0.08		
Validation			
MolProbity score	1.89		
Clashscore	13.42		
Poor rotamers (%)	0.29		
EMRinger score	3.43		